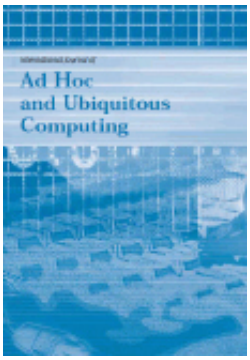

International Journal of Ad Hoc and Ubiquitous Computing

ISSN online: 1743-8233 - ISSN print: 1743-8225
https://www.inderscience.com/ijahuc

Optimal hybrid classifier with fine-tuned hyper parameter and improved fuzzy C means segmentation: skin cancer detection

Sreedhar Burada, Manjunathswamy Byranahalli Eraiah, M. Sunil Kumar

DOI: 10.1504/IJAHUC.2024.10061506

Article History:

Received:	26 December 2022
Last revised:	01 July 2023
Accepted:	11 September 2023
Published online:	18 January 2024

Optimal hybrid classifier with fine-tuned hyper parameter and improved fuzzy C means segmentation: skin cancer detection

Sreedhar Burada* and
Manjunathswamy Byranahalli Eraiah

Department of Computer Science and Engineering,
Don Bosco Institute of Technology,
Bengaluru, India
and
Visvesvaraya Technological University,
Belagavi, Karnataka, 560074, India
Email: sreedharburada1@gmail.com
Email: manjube24@gmail.com
*Corresponding author

M. Sunil Kumar

Department of Computer Science and Engineering,
School of Computing,
Mohan Babu University
Formerly; Sree Vidyanikethan Engineering College,
Tirupati, Andhra Pradesh 517102, India
Email: sunilmalchi1@gmail.com

Abstract: Skin cancer is regarded as the hazardous as well as widespread disease. Worldwide, there is been a 53% increment in present melanoma cases annually, and the mortality rate is also expected to be increasing in the coming decade. Hence, it is an urgent requirement to design a new early-detection model so that skin cancer can be more treatable without many complications. This work focuses on recognising skin cancer. The model includes the median filter (MF)-based pre-processing. The pre-processed image is subjected to a modified fuzzy C means (FCM)-based segmentation process. Finally, the recognition is done by employing a hybrid model with bi-LSTM and ANN. The proposed model's error rate was 0.091694, whereas the greatest error values for the other approaches were 0.20377 for BOA, 0.62192 for BRO, 0.170028 for ALO, 0.17168 for AOA, and 0.187915 for FIREFLY.

Keywords: skin cancer; modified FCM; bi-LSTM; improved CS-LDP; BRC-BOM algorithm.

Reference to this paper should be made as follows: Burada, S., Byranahalli Eraiah, M. and Kumar, M.S. (2024) 'Optimal hybrid classifier with fine-tuned hyper parameter and improved fuzzy C means segmentation: skin cancer detection', *Int. J. Ad Hoc and Ubiquitous Computing,* Vol. 45, No. 1, pp.52–64.

Biographical notes: Sreedhar Burada is pursuing his PhD from Don Bosco Institute of Technology, Bengaluru which was the research centre of Visvesvaraya Technological University, Belgavi, Karnataka. He completed his Master of Technology in computer science and engineering in JNTU Anantapur University. He completed his graduation in CSE, JNT University. His main research work relies on artificial neural networks, machine learning and deep neural networks.

Manjunathswamy Byranahalli Eraiah has graduated in Telecommunication Engineering from Visvesavaraya Technological University, Belgaum. He obtained his Masters of Engineering and Doctoral Degree in Computer Science and Engineering from UVCE, Bangalore University, Bangaluru. He has 15 years of teaching experience. Currently, he is working in the Department of Computer Science and Engineering, Don Bosco Institute of Technology. Bangalore. He has over 30 research papers to his credit. He received funds from AICTE. He has filed 4 Indian patents and one Australian Patent. His area of interest includes image processing, signal processing, and network security, cloud computing, IOT, and data science.

M. Sunil Kumar has completed his PhD in Computer Science and Engineering, S.V. University, Tirupati, MTech in Computer Science and Engineering from JNT University and BTech in Computer Science and Information Technology, JNT University. He is currently working as a

Professor and the Program Head, Department of Computer Science and Engineering, School of Computing, Mohan Babu University (erstwhile Sree Vidyanikethan Engineering College). His main research interests include software engineering, software architecture, machine learning, information retrieval and database management systems.

1 Introduction

The skin covering the body is an effective barrier against physical, chemical, and electromagnetic harm. It protects us from infections and contaminants and prevents moisture loss. Moreover, the skin has the capacity to lessen the adverse impacts of UV exposure owing to melanin pigment that absorbs UV light (Mohakud and Dash, 2022; Thurnhofer-Hemsi and Domínguez, 2021; Tumpa and Kabir, 2021). Melanoma, intraepithelial carcinoma, and other types of skin cancer all exist all over the world (Kumar et al., 2020; Adla et al., 2021; Togacar et al., 2021; Wei et al., 2020). According to statistics on cancer, skin cancer has a high death rate, with a mortality rate of individuals with skin tumours reaching up to 75% (Ali et al., 2021; Ashraf et al., 2020; Patil and Bellary, 2022; Adegun and Viriri, 2020).

The ABCDE rule: borders, asymmetry, diameter, evolving, and colour were a popular strategy for finding melanomas. To identify melanoma, these are the risk indicators that are used for tracking (Mignion et al., 2022; Adegun and Viriri, 2020; Senan and Jadhav, 2021). Dermoscopy was a magnetic resonance system that involves taking pictures of the epidermis with a light-amplifying tool and immersing fluid. This may increase the accuracy of malignant case diagnosis by 50% (Cheong et al., 2021; Rastghalam et al., 2021; Albahli et al., 2020).

Medical practitioners may not always be able to distinguish between benign and malignant malignancies when using visual imaging to diagnose skin cancer. Therefore, it was crucial to develop precise and efficient automatic classification methods for the identification and categorisation of skin malignancies (Mirbeik-Sabzevari et al., 2019; Monika et al., 2020; Wang et al., 2021).

AI had developed the capability to address these issues (Jaimes et al., 2015; Pennisi et al., 2016; Marchetti et al., 2017). The most reputable DL architectures, including RNN, DNN, and CNN are used in the medical industry to identify cancer cells. Skin cancer classification using these models is also accomplished satisfactorily (Yang et al., 2017; Ferris et al., 2015; Carrera et al., 2017; Hussain et al., 2016). Additionally, CNN is a deep technique that has previously produced exceptional outcomes in this area. The most widely used machine learning algorithm for extracting features and object classification, CNN, was employed in this model. To improve the accuracy of the outcomes, transfer learning was also applied in these fields in huge datasets (Alfed and Khelifi, 2017; Zhang et al., 2020; Tan et al., 2019; Xie et al., 2020).

The contributions are as follows:

- Modified fuzzy C mean (FCM)-based segmentation is introduced that assists in enhancing recognition accuracy.
- Determines a texture feature set that combines the CSLDP, LBP, LTP and GLCM features.
- Employs a hybrid model with ANN and bi-LSTM, in which the training will take place by a new BRC-BOM algorithm via tuning the optimal weights.

In this, Section 2 described existing schemes. Section 3 portrayed the detection of skin cancer: a new approach and Section 4 depicted modified FCM. Section 5 portrayed features. Section 6 depicted optimised BI-LSTM and ANN models. A Sections 7 and 8 describes the results.

2 Literature review

2.1 Related works

Mohakud and Dash (2022) developed an adaptive CNN in the year 2022, and it was afterward used for identifying the type of skin cancer. By deploying a suitable encoding scheme, the approach had used the GWO algorithm for optimising the CNN's parameters. By evaluating the model's performance against that of other algorithms, its efficacy was confirmed. The proposed model, according to simulation findings, was able to generate accuracy better to 98.33% which was about 4% and 1% higher than PSO and GA methods, correspondingly. Similar to the PSO method, the proposed model's testing loss was roughly 0.17%. The tentative findings unequivocally show that the suggested model outperforms previously reported, models.

Thurnhofer-Hems et al. (2021) presented a DL system for skin cancer detection. Five cutting-edge CNNs were trained using TL to provide both hierarchical and simple (two-level) classifiers that could find out between seven various types of moles. Data augmentation techniques are aided in the way that, studies were conducted with a sizable collection of skin images. Resultants showed that the chosen network is appropriate for the purpose because it produces high classification F-measures and accuracy with fewer false negatives. Even though the 1st level, or a double categorisation among non-nevi and nevi, had the better results, the plain model outperformed the two-level model.

Tumpa and Kabir (2021) created a NN in 2021 that was capable of accurately detecting and classifying melanoma. Dermoscopic images are first pre-processed using the MGIA to eliminate hairs, and the images are then enhanced. The OT technique was used to segment the pictures to remove skin lesions. The segmented images were then utilised to calculate many features like GLCM, LBP, and

ABCD that would be used to build a NN. The network was able to achieve a reliability of 97.7% and was determined to be more effective than other approaches since it used a lot more local features from the images.

Kumar et al. (2020) adopted a better technique to recognise three types of skin malignancies in their early stages in 2020. The proposed model is taken as input which is used to classify a skin sores image as either malicious or non-malignant tumours skin with its system. FCM was used to execute the picture segmentation in order to distinguish uniform image regions. The pre-processing was performed by adopting several filters for improving the imaging features, which were validated by merging the approaches of RGB colour space, LBP, and GLCM. Furthermore, the DE approach was used to train an ANN for classification. To get better outcomes, many features were precisely assessed. As indicated in the results, the uniqueness declared that DE-ANN performed better when varied to other conventional methods in respect of detection accuracy. The predicted outcome demonstrates that the suggested method accurately detected skin tumours with a 97.4% detection rate. In comparison to other conventional methodologies in the same domain, the results were very accurate.

An automatic model known as DLCAL-SLDC was created by Adla et al. (2021). The DLCAL-SLDC model's objective was to use dermoscopic pictures to identify and label different forms of skin tumours. To identify the afflicted tumour areas in the dermoscopy images pictures, a segmentation technique based on tall entropy was used. The CAL layer, was integrated into the CapsNet. The CSAE-based SSO technique, also known as the SSO-CSAE model, was used to perform the classification. With respect to several parameters, the suggested framework outperformed the competition with 98.50 percentage accuracy, 94.5% sensitivity, and 99.1% specificity.

To assure an effective DS tool, Togacar et al. (2021) developed a new model in 2021 that depends on auto-encoder, spiking, and CNNs. Images of 1,800 normal and 1,497 abnormal cells were used in the trials. The datasets were built using the auto-encoder model in the suggested method. The MobileNetV2 model, which is made up of residual blocks and spike networks, was trained on both the real and structured datasets. The study's categorisation success rate was 95%. Thus, it was discovered that the auto-encoder model and spike networks improved the performances.

A light weighted skin cancer identification model with feature discrimination depending upon the fine-grained categorisation principle was adopted by Wei et al. (2020) in 2020. The recommended scheme incorporates two typical lesion categorisation networks and discrimination network feature extraction modules. Numerous tests were deployed for validating the approach's performance and the outputs represents that the suggested model performed better than existing DL-based approaches.

A DCNN framework based on the DL approach was suggested by Ali et al. (2021) for the precise categorisation of malignant and benign skin tumours. The steps are as follows: first, apply a kernel or filter to reduce unwanted sounds and artefacts; second, standardise the input images and derive attributes that aid in precise categorisation; third, enrich the data with more images to increase classification accuracy. A few TL models were compared to the suggested DCNN model's performance. When compared to current TL methods, the proposed DCNN method's final results show that it is more trustworthy and resilient.

In 2023, Femil et al. have introduced the accurate detection of skin cancer. Dermoscopy images of skin lesions are initially acquired and processed by removing the noises with the aid of a Gabor filter. The pre-processed dermoscopy image is then divided into various sections using the cascaded fuzzy C-means (FCM) method, which increases the accuracy of cancer detection. Melanoma parameters are effectively extracted using a Gabor response co-occurrence matrix (GRCM). In order to effectively optimise the retrieved features, a hybrid particle swarm optimisation (PSO)-whale optimisation is then used.

In 2023, Dandu et al. the segmentation and classification of melanoma skin cancer is a challenge that the study attempts to solve. The fifth repeated skin cancer lesion is melanoma. The field of biomedical imaging and analysis has expanded. Recently, efforts for addressing the potential difficulties of malignant melanoma that may improve on epidermis have been promising, intriguing, and helpful. The accuracy of the suggested method is 90.6%.

2.2 Review

The automatic detection of skin diseases is a topic being worked on by a variety of researchers, institutions, and challenges. A variety of DL techniques were created to recognise dermatological disease, and they have been successful in a number of different disciplines. The performances could also be enhanced by utilising the right optimisation strategies. The impact on the training process makes it difficult for achieving maximum dependability and the least rate of time complexity at the similar time due to the disputes between several standards. A technique that is effective for identifying one skin lesion might not be effective for identifying others. Consequently, a fresh technique that is highly accurate is needed. Additionally, feature extraction methods can occasionally produce false findings. The images of skin cancer come in a variety of sizes and shapes, making it difficult to identify them with accuracy. According to this viewpoint, pre-processing is necessary for precise analysis. Low contrast from nearby tissues might occasionally present extra challenges and make it more difficult to correctly analyse skin cancer. Similar to this, a few signals that were not intended to be part of a picture but could interfere with a desirable result must be compromised. Therefore, all of this noise and artefacts should be eliminated during the pre-processing processes. Table 1 shows the review of conservative skin tumour models.

Table 1 Review of conservative skin tumour models

Author	*Method*	*Features*	*Challenges*	*Dataset used*
Mohakud and Dash (2022)	• CNN	• High accuracy • Testing loss is low	• Improve the training size • Also, consider the regularisation rate	• International skin imaging collaboration (ISIC) dermoscopic skin cancer image dataset
Thurnhofer-Hemsi and Domínguez (2021)	• CNN	• Recall is high • F-measure is maximised	• Need more accurate prediction	• The HAM10000 dataset
Tumpa and Kabir (2021)	• ANN	• Higher accuracy • Maximal sensitivity	• Improve the feature extraction	• PH^2 dermoscopic image database
Kumar et al. (2020)	• DE-ANN	• Highest specificity	• Improve the performance	• Skin cancer image datasets namely HAM10000 and PH^2
Adla et al. (2021)	• DLCAL-SLDC	• High sensitivity • Maximum specificity	• It is necessary to test in the large-scale dataset	• Benchmark ISIC dataset
Togacar et al. (2021)	• CNN	• High sensitivity	• Consider the performance of RAE and RRES	• ISIC skin cancer dataset
Wei et al. (2020)	• DL model	• It is more effective	• Improve the accuracy	• ISBI 2016 dermoscopy image
Ali et al. (2021)	• DCNN	• Higher training rate • It is more reliable and robust	• Varied lesion types cannot be determined	• HAM10000 dataset

Figure 1 Pictorial representation of adopted skin tumour detection model (see online version for colours)

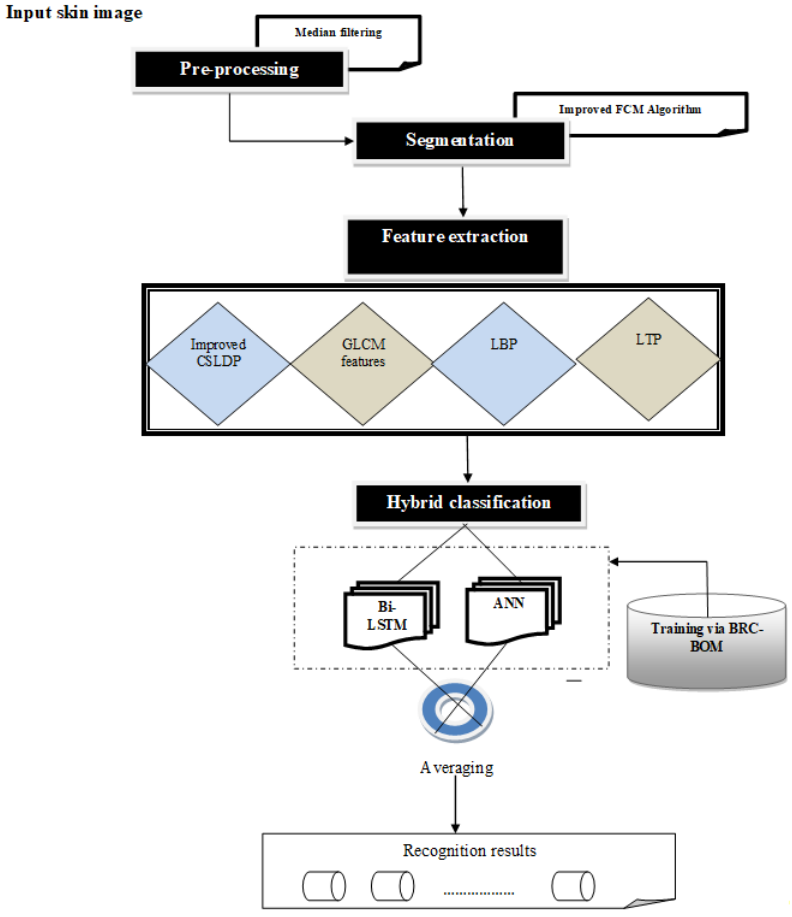

3 Recognition of skin cancer: a new proposed architecture

Skin cancer recognition is the most crucial model, which reduces the death rate. The proposed recognition model includes the following procedure:

- The input image *im* is pre-processed using median filter (MF) in the initial stage.
- Introduces a modified FCM is for segmenting the image.
- After this, features like Improved CSLDP, LBP, LTP, and GLCM features are extracted from the segmented image.
- Further, recognition takes place by the hybrid classifier with combining models like bi-LSTM and ANN, respectively.
- The training of the hybrid model is performed by BRC-BOM model via tuning the optimal weights. Figure 1 shows the representation of the proposed framework.

3.1 Pre-processing

Here, we deploy MF to pre-process *im*. Pre-processing is necessitated to enhance the image quality. MF (https://en.wikipedia.org/wiki/Median_filter): a digital nonlinear filter technique known as MF is used frequently to get rid of noise from *im*. This kind of noise diminution is a general pre-processing method for improving the outcomes of processing. MF is greatly employed to process images and in definite cases, it maintains edges while lessening noise. The outcomes from MF are termed as (im^{mf}).

4 Modified FCM-based segmentation

The results from MF are based on the modified FCM for separating im^{mf}.

4.1 Modified FCM model (MFCM)

Segmentation is the process of separating the ROI and non-RoI parts of the diseased region. This work takes account of the FCM process with the modified procedure to evolve the segmentation outcome. The objectives for modelling the MFCM scheme are shown in equation (1) (Kahali et al., 2018).

$$G(N,U)=\sum_{k=1}^{C}\sum_{i=i}^{M}v_{ik}^{n}\left(1-e^{-\frac{\|y_i-\mu_k\|^2}{2\sigma_k^2}}\right) \tag{1}$$

In equation (1), $n > 1$ signifies the fuzziness coefficient; v_{ik} indicates the membership degree of y_i in cluster k, i.e., $\sum_{k=1}^{C}v_{ik}=1$; and $V(y_i)$ signifies the uncertainty of class (the limits of obtained images are imprecise owing to the existence of noise or biased volume effect. Here, the pixels at the border are as includes the higher value of class entropy or uncertainty) linked with the specified intensity of the pixel y_i.

As per MFCM, the entropy-based FCM is modelled as in equation (2). Equation (3) shows the entropy formula, wherein, p_{ik} refers to the probability of pixel's intensity, σ_s and μ_k refers to standard deviation and mean of intensity for k^{th} class.

$$G(N,U)=\sum_{k=1}^{C}\sum_{i=1}^{M}v_{ik}^{n}\left(1-e^{-\frac{\|y_i-\mu_k\|^2}{2\sigma_k^2}}\right)+\sum_{i=1}^{M}V(y_i) \tag{2}$$

$$V(y_i)=\sum_{k=1}^{C}p_{ik}\log p_{ik} \tag{3}$$

The modified FCM image is represented as im^{MFCM}.

5 Extracting ICS-LDP, LBP, LTP, and GLCM features

Texture features are the major concern in the image input, which gives pattern-based information from the region. In this way, from the segmented image im^{MFCM}, the ICS-LDP, LBP, LTP, and GLCM features are derived in this paper. Lastly, the combined set of features is subjected to classification. The description of each pattern features is as follows:

5.1 ICS-LDP features

LBP (Xue et al., 2011) could be measured as a 1st order localised pattern that is the binary outcome of 1st order derivative images. CS-LBP creates many small feature sets when compared to LBP, however, it is moreover a 1st order LDP in a centre symmetrical direction and it disregards the centre pixel data. As the 1st order derivative patterns are unable to describe more data and the higher order LDP in Zhang et al. (2010) and Zhao et al. (2010) creates much longer feature sets, which is not appropriate for backdrop modelling. Here, a new CS-LDP model is proposed that is a 2nd order LDP in a centre symmetrical direction. CS-LDP model could confine more detailed info while containing a similar feature length to CS-LBP. Conventionally, it is stated as in equation (4), in which, h_d signifies the grey value of the colour pixel ($z_d g_d$), h_i and $h_{i+(n/2)}$ refers to values of nearby pixels in the centre symmetrical direction. And, t refers to the threshold

$$f^{CS-LDP}=\sum_{i=0}^{(n/2)-1}t\left[\left(h_i-h_d\right)\cdot\left(h_d-h_{i+(n/2)}\right)\right]2^i \tag{4}$$

As per the improved feature, CS-LDP is defined as in equation (5).

$$f^{ICS-LDP}=q(z,g)\sum_{i=0}^{(n/2)-1}t\left[\left(h_i-h_d\right)\cdot\left(h_d-h_{i+(n/2)}\right)\right]2^i \tag{5}$$

In equation (5), $q(z, g) = [q_z, q_g]$ is evaluated at every pixel position, the gradient vector $q(z, g)$ is accumulated in a gradient map with two elements $q_z(z, g)$ and $q_g(z, g)$ corresponds to 2 sub-images based on equation (6).

$$t(z_1, z_2) = \begin{cases} 0 & \text{if } z_1 \cdot z_2 > 0 \\ 1 & \text{if } z_1 \cdot z_2 \le 0 \end{cases} \tag{6}$$

Table 2 GLCM features

S. no.	*Features*	*Arithmetical term*
1	Energy	$E = \sum_{\omega}\sum_{\xi} \upsilon_{\omega\xi}^2$ here $\upsilon_{\omega\xi}$ is the $(\omega, \xi)^{\text{th}}$ entry
2	Entropy	$Et = -\sum_{\omega}\sum_{\xi} \upsilon_{\omega\xi} \log_2 \upsilon_{\omega\xi}$
3	Difference entropy	$DE = \sum_{\omega=0}^{N_v-1} \upsilon_{x-y}(\omega) \log\{\upsilon_{x-y}(\omega)\}$
4	Contrast	$Con = \sum_{\omega}\sum_{\xi} (\omega - \xi)^2 \upsilon_{\omega\xi}$
5	Sum variance	$SV = \sum_{\omega=2}^{2N_v} (\omega - SE)^2 s_{x+y}(\omega)$
6	Correlation	$Cor = \frac{\sum_{\omega}\sum_{\xi} (\omega\xi)\upsilon_{\omega\xi} - \mu_x\mu_y}{\sigma_x\sigma_y}$, where σ_x, σ_y, μ_x, μ_y are the std deviations and mean of υ_x, υ_y
7	Variance	$Var = \sum_{\omega}\sum_{\xi} (\omega - \mu)^2 \upsilon_{\omega\xi}$, where μ denotes the mean of $\upsilon_{\omega\xi}$
8	IMC 1	$IMC\,1 = \frac{hxy - hxy1}{\max\{hx, hy\}}$
9	Sum average	$SA = \sum_{\omega=2}^{2Nv} \omega \cdot \upsilon_{x+y}(\omega)$, where N_v indicates the varied grey levels in image
10	Homogeneity	$Hom = \sum_{\omega}\sum_{\omega} \frac{1}{1 + (\omega - \xi)} \upsilon_{\omega\xi}$
11	Sum entropy	$SE = \sum_{\omega=2}^{2N_v} \upsilon_{x+y}(\omega) \log\{\upsilon_{x+y}(\omega)\}$
12	Difference variance	$DV = variance\ of\ \upsilon_{\omega x-y}$
13	MCC	$MCC = \sum_{k} \frac{g(\omega, k)g(b, k)}{g_x(\omega)g_y(k)}$
14	IMC 2	$IMC\,2 = \sqrt{(1 - \exp[-2.0[hxy1 - hxy]])}$, , where $hxy = -\sum_{\omega}\sum_{\xi} \upsilon_{\omega\xi} \log_2 \upsilon_{\omega\xi}$ and $hxy1 = -\sum_{\omega}\sum_{\xi} \upsilon_{\omega\xi} \log_2\{\upsilon_x(\omega)\upsilon_y(\xi)\}$

5.2 GLCM features

It is used to assess the spatial link amid the pixels (Arabi et al., 2016). The constraint in GLCM is specified in Table 2.

5.3 LBP features

The LBP (Fan and Hung, 2014) is shown with simplicity in a variety of comparison investigations. To extract the differential features between a definite reference pixel and its surrounding radius R, the basic LBP is used. For a pixel at (q_e, r_e), the resulting LBP is written as in equation (7), where $\bar{i}$ denotes the geometric mean of nearby pixels, i_e and i_P implies greyscale values of the central pixel and its surrounding pixels P with R.

$$LBP_{P,R}(q_e, r_e) = \sum_{P=0}^{P-1} s * 2^P \tag{7}$$

5.4 LTP features

The LTP (Mondal et al., 2021) has shown promising results for segmenting and analysing images. Here, a novel adaptive LTP technique enables pattern extraction for skin tumour identification. LTP eliminates light variations while maintaining the necessary picture appearance data. LTP advances the field of pattern extraction significantly since it is more noise invariant than LBP. The relationships of 'greater than, equal to, and less than' amongst a pixel and its neighbouring pixels are reflected by LTP.

The two standard values (0, 1) in LTP are expanded to three ternary code (–1, 0, +1) using a threshold. The number 1 is set as the threshold. The grey values in breadth about the grey level of the middle pixel, o_c is set to '0' and grey values beyond $o_c + \Delta$ is set to +1 and grey values beyond $o_c - \Delta$ is set to –1. A three-valued operation is employed for the depiction of LTP code as shown in equation (8).

$$\phi(o_p, o_c, \Delta) = \begin{cases} +1; & o_p >= o_c + \Delta \\ 0; & |o_p - o_c| < \Delta \\ -1; & o_p <= o_c < \Delta \end{cases} \tag{8}$$

The derived ICS-LDP, LBP, LTP and GLCM are totally termed as f.

6 Optimised bi-LSTM and ANN models: the hybrid model for recognition

The extracted feature (f) is then offered as input to a hybrid method which contains two classifiers like bi-LSTM and ANN. The working principle is the extracted feature set is individually subjected to bi-LSTM and ANN models, respectively. The results from them are median to achieve the final outcome. Here, the training will be performed by the optimisation algorithm, for which a new BRC-BOM algorithm is introduced in this work, which is explained in the subsequent section.

6.1 Bi-LSTM

The gates namely, forget, input, and output are three gating components that form an LSTM (Zhou et al., 2019). Each neuron in LSTM can be calculated independently using equations (9)–(13), assuming that the incoming sequence is $(p_1, p_2, \ldots, p_3)$.

$$l_t = G\left(w_l \times [x_{t-1}, p_t] + o_l\right) \tag{9}$$

$$m_t = G\left(w_m \times [x_{t-1}, p_t] + o_m\right) \tag{10}$$

$$n_t = G\left(w_n \times [c_t, x_{t-1}, p_t] + o_n\right) \tag{11}$$

$$c_t = m_t \times c_{t-1} + l_t \times \tan x\left(w_c \times [x_{t-1}, p_t]\right) \tag{12}$$

$$x_t = n_t \times \tan x(c_t) \tag{13}$$

Here,

- t = time
- l_t, m_t, n_t = input of input and output gate
- G = sigmoid function
- p_t = LSTM neuron input
- o_l, o_m, o_n = offset vectors
- x_t = output of hidden layer
- w_l, w_m, w_n = weight matrices of input and output cell.

6.2 ANN

NN (Mohan et al., 2016) is employed to discover the harshness of the disease. Equations (14), (15) and (16) establish the network model, wherein, $\hat{w}e_{(\tilde{b}i)}^{(HI)}$ implies to weight (bias) to i^{th} hidden neuron, i implies to hidden neuron, $in_{(n)}$ implies to count of input neurons, $HI(n)$ implies count of hidden neurons, $\hat{w}e_{(ik)}^{(o)}$ implies to output weight from i^{th} hidden neuron to k^{th} layer, $\hat{w}e_{(\tilde{b}k)}^{(o)}$ implies to weight (output bias) to k^{th} layer, NF implies to activation function, $\hat{w}e_{(li)}^{(HI)}$ represents to weight from l^{th} input to i^{th} hidden neuron and, OU_k and $\overline{OU}_k$ represents actual output and predicted output.

$$\overline{HO}^{(HI)} = NF\left(\hat{w}e_{(\tilde{b}i)}^{(HI)} + \sum_{l=1}^{in_{(n)}} \hat{w}e_{(li)}^{(HI)}(f)\right) \tag{14}$$

$$\overline{OU}_k = NF\left(\hat{w}e_{(\tilde{b}k)}^{(o)} + \sum_{i=1}^{HI(n)} \hat{w}e_{(ik)}^{(o)} \overline{HO}_i^{(HI)}\right) \tag{15}$$

$$Err = \underset{\left\{\hat{w}e_{(\tilde{b}i)}^{(HI)}, \hat{w}_{(li)}^{(HI)}, \hat{w}e_{(\tilde{b}k)}^{(o)}, \hat{w}e_{(ik)}^{(o)}\right\}}{\arg\min} \sum_{k=1}^{O(n)} \left|OU_k - \overline{OU}_k\right| \tag{16}$$

The bi-LSTM and ANN outputs are averaged to obtain final outcome.

Objective: the intention is to lower error as in equation (17).

$$Objective = \min(Err) \tag{17}$$

The weights of bi-LSTM (w) and ANN (we) are optimally selected by the BRC-BOM scheme. Table 3 describes the hyper parameters of classifiers.

Table 3 Classifier hyperparameters

Methods	*Hyperparameters*
ANN	dense layer size = 100, activation = 'relu'
	dense layer 2 size = 3, activation = 'softmax
	loss = 'sparse_categorical_crossentropy'
	optimiser = 'rmsprop'
Bi-LSTM	filter size = 128
	activation = 'sigmoid'
	loss = 'sparse_categorical_crossentropy
	optimiser = 'adam'
Bi-GRU	filter size = 64, activation = 'relu'
	dense layer size = 3, activation = 'softmax'
	loss = 'sparse_categorical_crossentropy'
	optimiser = 'rmsprop'
SVM	C = 0.03
	kernel = 'linear

6.3 BRC-BOM scheme for training: tuning the optimal weights

Here, we combine the theories of BOA (Arora and Singh, 2019) and BRO (Farshi, 2021) to form BRC-BOM. Hybrid schemes results in better outcomes in terms of convergence speed (Beno et al., 2014), which is validated in the results section by comparing the model with existing algorithms. To overcomes the limitations such as low convergence and fall into the local optima. The proposed model is used.

BOA was impacted by how butterflies scavenge and mate. In particular, scents with unique scents in each butterfly are the distinguishing feature of BOA, which is formulated as in equation (18), where the power exponent α, modality sensory index is referred by $s \in (0, 1)$, the stimuli intensity is referred by l, and the index refers to the intensity of the stimulus.

$$q = sl^{\alpha} \tag{18}$$

The three phases in BOA are described as follows:

1 Initialisation: The constraints, solution space and objectives are specified.

2 Iteration: Two diverse search schemes: global and local search were deployed in this iteration.

Conventionally, the global searching is shown in equation (19), here, ψ_i^t represents i^{th} position at

iteration t and G_{best} represents the global best position. Specifically, δ_i represents i^{th} butterfly's scent.

$$\psi_i^{t+1} = \psi_i^t + \left(r^2 \times G_{best} - \psi_i^t\right) \times \delta_i \tag{19}$$

As per BRC-BOM, the global search position is modelled by combining equation (20) of BRO to form equation (23).

$$\psi_i^{t+1} = r(ud - ld) + ld \tag{20}$$

$$\psi_i^{t+1} = \left[r(ud - ld) + ld\right] + \left(r^2 \times G_{best} - \psi_i^t\right) \times \delta_i \tag{21}$$

$$\psi_i^{t+1} = r(ud - ld) + r^2 G_{best}\delta_i - \psi_i^t \delta_i + ld \tag{22}$$

$$\psi_i^{t+1} = r\left[(ud - ld) + rG_{best}\delta_i\right] - \psi_i^t \delta_i + ld \tag{23}$$

In equation (23), $\delta_i \in 0, 1$ and r refers to random integer computed via the logistic map.

The position of the butterflies is used for modelling the local search, as shown in equation (24), wherein, and denotes ψ_j^t and ψ_j^t butterflies.

$$\psi_i^{t+1} = \psi_i^t + \left(r^2 \times \psi_j^t - \psi_k^t\right) \times \delta_i \tag{24}$$

Moreover, a switch probability is assigned. As per BRC-BOM, the final solution is then passed through a Lévy flight. A Lévy flight is a random walk in which the step lengths follow a probability distribution with heavy tails called the Lévy distribution. When a walk is known as having more dimension, the directions in which the steps are taken are isotropic.

3 Termination: BOA terminates when the utmost iteration is reached. The BRC-BOM is in Algorithm 1.

Algorithm 1 BRC-BOM model

```
Initialising population
Calculate the intensity of stimuli
When stopping criteria does not meet
    for each population do
        Calculate scent for BF as in equation (18)
    end for
    Discover best BF
    for every butterfly BF in the populace do
    Consider an arbitrary integer denoted by ra
        if r < pr
            Update position as per proposed equation (23)
        else
            Update position as per equation (24)
        end if
        Apply Lévy flight concept (proposed)
    end for
    update α
end while
```

Table 4 shows the algorithm parameters.

Table 4 Parameters of algorithm

Methods	*Parameters*
BOA	c = 0.01, p = 0.8, alpha = (0.1, 0.3)
BRO	threshold = 3
AOA	alpha = 5, miu = 0.5, moa_min = 0.2, moa_max = 0.9
Firefly algorithm	gamma = 1, beta_base = 1, alpha = 0.2, alpha_damp = 0.99, delta = 0.05, m = 2

7 Results and discussion

7.1 Simulation setup

Python was used to execute the suggested based on skin cancer detection. The proposed BRC-BOM method was examined over the conventional methodologies including BOA, BRO, ALO, AOA, and FF. Similarly, the assessment was conducted, in terms of, positive metrics (accuracy, precision, sensitivity, and specificity), negative metrics (FNR and FPR), and other metrics (F-measure, MCC, and NPV). The skin cancer images are displayed in Figure 2.

7.2 Dataset description

The dataset was collected from (https://www.fc.up.pt/addi/ph2%20database.html),

> "The dermoscopic images were obtained at the Dermatology Service of Hospital Pedro Hispano (Matosinhos, Portugal) under the same conditions through the Tuebinger mole analyzer system using a magnification of 20×. They are 8-bit RGB colour images with a resolution of 768 × 560 pixels. This image database contains a total of 200 dermoscopic images of melanocytic lesions, including 80 common nevi, 80 atypical nevi, and 40 melanomas. The PH^2 database includes medical annotation of all the images namely medical segmentation of the lesion, clinical and histological diagnosis, and the assessment of several dermoscopic criteria (colours; pigment network; dots/globules; streaks; regression areas; blue-whitish veil)."

7.3 Analysis of a positive metrics

The analysis on positive measures for the BRC-BOM model over the standard approaches, namely, BOA, ALO, BRO, AOA, and FIREFLY are specified in Figure 3. When observing those figures, the developed strategy surpassed the established approaches in terms of detection accuracy. As shown in Figure 3(a), the suggested model has the maximum detection accuracy at 90% learning percentage is (~) 97.42%, although the other approaches seemed to have the lowest detection accuracy, such as BOA is 77.18%, ALO is 79.02%, BRO is 78.93%, AOA is 80.47% and FIREFLY is 81.16%, respectively.

Figure 2 Skin cancer detection images (see online version for colours)

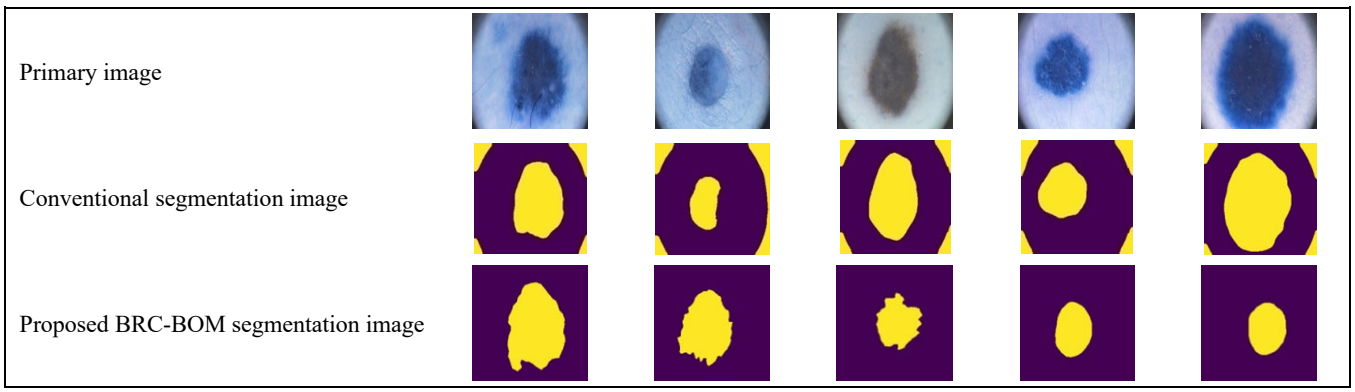

Moreover, the recommended method received the greatest value for precision, specificity, and sensitivity. Particularly, the models' FIREFLY, BOA, ALO, BRO, and AOA reached the minimum specificity of 69.73%, 74.74%, 77.15%, 78.98%, and 90.86%, whilst the suggested model yields the specificity of 95.54%, in the 80% of learning percentage. The developed method accomplished its highest precision at 90%of the learning percentage is 98.59%. Finally, looking at Figure 3(d), the presented approach achieved a sensitivity of 94.67%, at the 90% learning percentage, exceeding BOA, BRO, ALO, AOA, and FIREFLY, which each have a sensitivity of 81.52%, 84%, 86.92%, and 87.05%. Thus, from the investigation, it is known that the suggested BRC-BOM scheme is substantially more reliable for detecting skin cancer with maximal accuracy and precision rate.

Figure 3 Analysis of, (a) accuracy (b) specificity (c) precision (d) sensitivity (see online version for colours)

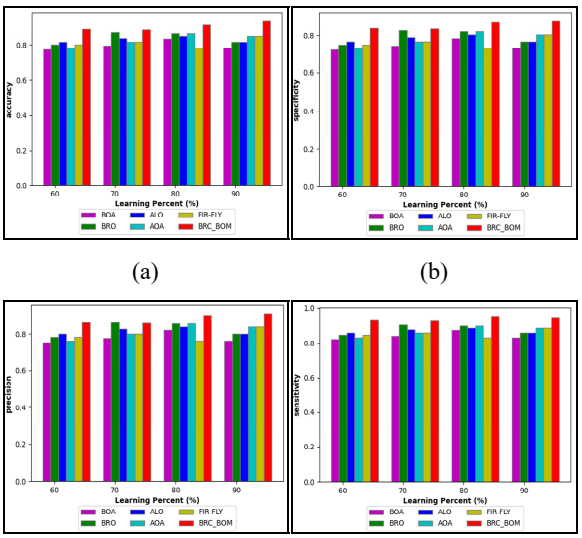

(a) (b)

(c) (d)

7.4 Analysis of a negative measure

Figure 4 shows the suggested BRC-BOM method's negative metrics (FNR and FPR) with those traditional approaches. From Figures 4(a) and 4(b), the developed method maintained the lowest FNR and FPR values than the other methods in the overall learning percentage. At 90%of the learning percent, the recommended method created an FNR of 0.034, this is considerably low than the established methods including, BOA (0.158), BRO (0.126), ALO (0.127), AOA (0.110) and FIREFLY (0.112). Considering Figure 4(b), the minimum FPR recorded by the suggested model at the 80% of learning rate is 0.11, which is more desirable than BOA, BRO, ALO, AOA, and FIREFLY. The suggested BRC-BOM methodology demonstrated its reliability in identifying skin cancer more precisely with low error.

Figure 4 Analysis of, (a) FNR (b) FPR (see online version for colours)

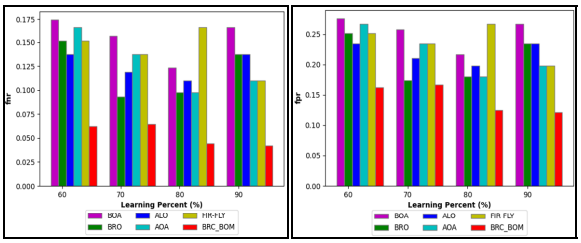

(a) (b)

7.5 Analysis of other measures

Figure 5 represented the other metrics of the suggested BRC-BOM model is varied to the conventional models. The other measure has to be maximum in the adopted model for its effective performance. From Figure 5(a), the suggested technique obtained the F-measure of 98.36%, in contrast, the other current methods scored the lowest F-measure including BOA = 77.15%, ALO = 79.89%, AOA = 80%, and FIREFLY = 81.83%, respectively. Subsequently, the suggested model with respect of MCC has obtained a better performance of 92.17% (in the 80% of the learning percentage) this is superior to BOA, ALO, AOA, FIREFLY, and BRO respectively. Further, the proposed model offers a greater NPV compared to other traditional methods like BOA, BRO, ALO, AOA, and FIREFLY for a learning percentage of 70%. Similarly, the NPV analysis of the BRC-BOM is 94.97%, which is desirable than BOA is 74.82%, BRO is 76.47%, ALO is 77%, AOA is 83.92%, FIREFLY is 84.89%. As a result, the suggested BRC-BOM

strategy delivered beneficial outcomes and enhanced the detection accuracy for skin cancer.

Figure 5 Analysis on, (a) F-measure (b) MCC (c) NPV (see online version for colours)

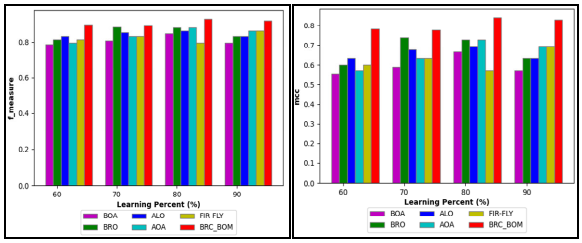

(a) (b)

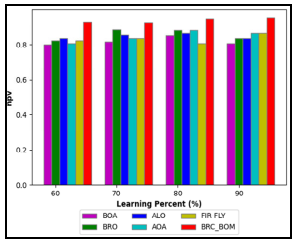

(c)

7.6 *Statistical analysis*

Table 5 describes the statistical analysis of the proposed BRC-BOM technique against the traditional methods (BOA, BRO, ALO, AOA, and FIREFLY). Reviewing the Mean scenario, the proposed model acquired an error rate of 0.091694, even though the other methods scored the highest error value of BOA is 0.20377, BRO is 0.162192, ALO is 0.170028, AOA is 0.17168 and FIREFLY is 0.187915. Based on the worst-case scenario, the lowest error value acquired by the suggested model is 0.095916 this is better when compared to BOA (0.225307), BRO (0.200114), ALO (0.183577), AOA (0.216857) and FIREFLY (0.216857). The evaluation has shown that the adopted BRC-BOM model ensures a lowest error value than the other relevant previous systems.

Table 5 Statistical analysis

	Best	*Worst*	*Mean*	*Median*	*Standard deviation*
BOA	0.167245	0.225307	0.20377	0.211264	0.022208
BRO	0.129905	0.200114	0.162192	0.159376	0.030281
ALO	0.151111	0.183577	0.170028	0.172711	0.014071
AOA	0.135174	0.216857	0.17168	0.167344	0.031378
FIREFLY	0.151111	0.216857	0.187915	0.191845	0.024289
BRC-BOM	0.060951	0.113992	0.091694	0.095916	0.021836

7.7 *Classifier comparison*

Table 6 depicts the classifier analysis over the other classifiers such as bi-LSTM, ANN, bi-GRU, SVM, CNN (Thurnhofer-Hemsi and Domínguez, 2021), and NN (Tumpa and Kabir, 2021). Here, the proposed approach recorded the greatest detection accuracy with low FPR and FNR. Particularly, the accuracy of the suggested method is 93.90%, excessively high against the bi-LSTM = 81.38%, ANN = 83.01%, bi-GRU = 76.36%, SVM = 69.13%, CNN = 79.56%, and NN = 76.11%, respectively. The FNR, MCC, sensitivity, and F-measure of the suggested work are 0.042361, 82.61%, 95.06%, and 91.73%. Furthermore, the suggested BRC-BOM method obtained an FPR of 0.121, which is preferable, then the following methods: bi-LSTM (0.222318), ANN (0.133803), bi-GRU (0.291667), SVM (0.376286), CNN (0.173517) and NN (0.25002), respectively.

7.8 *Ablation study*

Table 7 shows the ablation study of the suggested BRC-BOM work, model without optimisation, and model without segmentation. The proposed method attained a detection accuracy of 93.90%, the model without BRC-BOM is 87.86%, and the model without segmentation is 74.88%. Similarly, the F-measure of the proposed technique, model without BRC-BOM, and model without segmentation is 91.73%, 88.28%, and 74.43%. Consequently, the suggested method, model without BRC-BOM and model without segmentation acquired the FPR of 0.121, 0.137703, and 0.22595.

7.9 *Convergence analysis*

Figure 6 portrays the convergence BRC-BOM analysis of the suggested method in contrast to the established methodologies which include BOA, BRO, ALO, AOA, and FIREFLY by modifying the iterations to 10, 20, 30, 40, and 50, respectively. In the first iteration, the high error rate observed in the proposed work is (~) 1.0925, nevertheless, it began to converge from iteration 10 and scored the lower error value of 1.0751 in the 50th iteration. The maximum error rate is acquired by the FIREFLY (1.07743) and BOA (1.07742). Altogether, it is demonstrated that the proposed BRC-BOM provides improved skin cancer detection with decreased error.

Figure 6 Convergence study of the proposed BRC-BOM model vs. conventional approaches (see online version for colours)

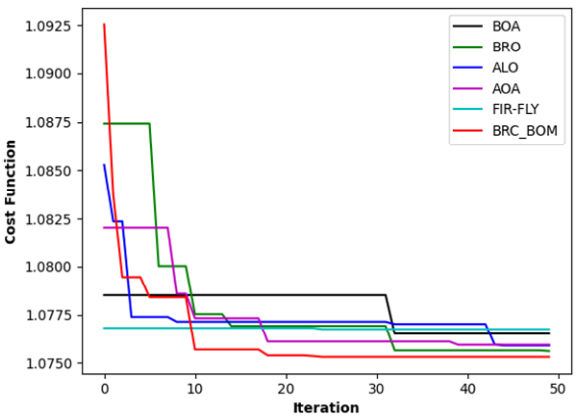

Table 6 Classifier comparison

	BRC-BOM	*Bi-LSTM*	*ANN*	*Bi-GRU*	*SVM*	*CNN (Thurnhofer-Hemsi and Domínguez, 2021)*	*NN (Tumpa and Kabir, 2021)*
Sensitivity	0.950639	0.845145	0.789364	0.837675	0.777584	0.76581	0.74998
MCC	0.826124	0.625166	0.658863	0.540881	0.400576	0.593027	0.51604
Accuracy	0.939049	0.813802	0.830163	0.763601	0.691339	0.795696	0.761166
FNR	0.042361	0.154855	0.210636	0.162325	0.222416	0.23419	0.25002
F-measure	0.917304	0.829365	0.813418	0.751753	0.688895	0.791844	0.727629
Specificity	0.879	0.777682	0.866197	0.708333	0.623714	0.826483	0.769445
NPV	0.950304	0.813351	0.823197	0.853984	0.78149	0.77405	0.806106
FPR	0.121	0.222318	0.133803	0.291667	0.376286	0.173517	0.230555
Precision	0.907826	0.814163	0.838983	0.681818	0.618365	0.81971	0.70657

Table 7 Ablation study

	BRC-BOM	*Proposed without BRC-BOM*	*Proposed without segmentation*
Accuracy	0.939049	0.878683	0.748843
NPV	0.950304	0.886374	0.733333
Sensitivity	0.950639	0.894344	0.724138
Precision	0.907826	0.871712	0.76581
FNR	0.042361	0.105656	0.275862
MCC	0.826124	0.757364	0.498666
Specificity	0.879	0.862297	0.77405
FPR	0.121	0.137703	0.22595
F-measure	0.917304	0.882883	0.744391

7.10 Analysis on dice coefficient

The dice coefficient analysis is shown in Table 8. A statistical method called the dice coefficient assesses how similar two sets of data are. Perhaps the most often used tool for evaluating picture segmentation methods is this index. The dice coefficient of the suggested technique is high varied to the traditional methods.

Table 8 Dice coefficient analysis

Image	*Proposed model*	*Conventional model*
image1	0.743716	0.681643
image2	0.711871	0.64047
image3	0.69143	0.629062
image4	0.692676	0.636665
image5	0.691665	0.627785

7.11 Computational time

The computational time analysis is given in Table 9. The computational analysis of the suggested method is less (~56.36) than the other conventional schemes such as BOA, BRO, ALO, AOA and FIREFLY. Furthermore, it proved the efficiency of the suggested method.

Table 9 Computational time analysis

Models	*Time*
BOA	70.53
BRO	79.57
ALO	101.57
AOA	107.97
FIREFLY	92.32
Proposed model	56.36

8 Conclusions

This article introduced a novel technique for detecting skin cancer. The work exploited MF for pre-processing. Further, modified FCM was used for segmenting images. Then, features like LBP, GLCM, LTP, and improved CS-LDP were derived. At last, detection was done by employing two models namely, bi-LSTM and ANN, whose results were fused to get the detected outcomes. Reviewing the Mean case, the suggested model attained the error value of 0.091694, even though the other methods scored the highest error value of BOA was 0.20377, BRO was 0.162192, ALO was 0.170028, AOA was 0.17168 and FF was 0.187915. Based on the worst-case, the lowest error value acquired by the suggested model was 0.095916 this is better when compared to BOA (0.225307), BRO (0.200114), ALO (0.183577), AOA (0.216857) and FF (0.216857). The diagnosis of skin cancer disorders and artificial intelligence are likely to become closely related in the future.

References

Adegun, A. and Viriri, S. (2020) 'Deep learning-based system for automatic melanoma detection', in *IEEE Access*, Vol. 8, pp.7160–7172, DOI: 10.1109/ACCESS.2019.2962812.

Adegun, A. and Viriri, S. (2020) 'FCN-based DenseNet framework for automated detection and classification of skin lesions in dermoscopy images', in *IEEE Access*, Vol. 8, pp.150377–150396, DOI: 10.1109/ACCESS.2020.3016651.

Adla, D., Reddy, G.V.R., Nayak, P. et al. (2021) 'Deep learning-based computer aided diagnosis model for skin cancer detection and classification', *Distrib. Parallel Databases* https://doi.org/10.1007/s10619-021-07360-z.

Albahli, S., Nida, N., Irtaza, A., Yousaf, M.H. and Mahmood, M.T. (2020) 'Melanoma lesion detection and segmentation using YOLOv4-DarkNet and active contour', in *IEEE Access*, Vol. 8, pp.198403–198414, DOI: 10.1109/ACCESS.2020.3035345.

Alfed, N. and Khelifi, F. (2017) 'Bagged textural and color features for melanoma skin cancer detection in dermoscopic and standard images', *Expert Systems with Applications*, December, Vol. 9030, pp.101–110.

Ali, M.S., Miah, M.S., Haque, J., Rahman, M.M. and Islam, M.K. (2021) 'An enhanced technique of skin cancer classification using deep convolutional neural network with transfer learning models', *Machine Learning with Applications*, Vol. 5, pp.1–8.

Arabi, P.M., Joshi, G. and Deepa, N.V. (2016) 'Performance evaluation of GLCM and pixel intensity matrix for skin texture analysis', *Perspectives in Science*, September, Vol. 8, pp.203–206.

Arora, S. and Singh, S. (2019) 'Butterfly optimization algorithm: a novel approach for global optimization', *Soft Comput*., Vol. 23, pp.715–734 https://doi.org/10.1007/s00500-018-3102-4.

Ashraf, R. et al. (2020) 'Region-of-interest based transfer learning assisted framework for skin cancer detection', in *IEEE Access*, Vol. 8, pp.147858–147871, DOI: 10.1109/ACCESS.2020.3014701.

Beno, M.M., Valarmathi, I.R., Swamy, S.M. and Rajakumar, B.R. (2014) 'Threshold prediction for segmenting tumour from brain MRI scans', *International Journal of Imaging Systems and Technology*, Vol. 24, No. 2, pp.129–137 https://doi.org/10.1002/ima.22087.

Carrera, C., Scope, A., Dusza, S.W., Argenziano, G. and Marghoob, A.A. (2017) 'Clinical and dermoscopic characterization of pediatric and childhood melanomas. Multicenter study of 52 cases', *Journal of the American Academy of Dermatology*, 9 October, Vol. 38, No. 2, pp.278–288.

Cheong, K.H., Tang, K.J.W., Zhao, X., Koh, J.E.W., Faust, O., Gururajan, R., Ciaccio, E.J., Rajinikanth, V. and Acharya, U.R. (2021) 'An automated skin melanoma detection system with melanoma-index based on entropy features', *ScienceDirect*, Vol. 41, No. 3, pp.997–1012.

Dandu, Ravi, M., Murthy, V. and Kumar, Y.B.R. (2023) 'Transfer learning for segmentation with hybrid classification to detect melanoma skin cancer', *Heliyon*, Vol. 9, No. 4, pp.1–8.

Fan, K-C. and Hung, T-Y. (2014) 'A novel local pattern descriptor – local vector pattern in high-order derivative space for face recognition', *IEEE Transactions on Image Processing*, July, Vol. 23, No. 7, pp.2877–2889.

Farshi, T.R. (2021) 'Battle royal optimization algorithm', *Neural Comput. & Applic*., Vol. 33, pp.1139–1157 https://doi.org/10.1007/s00521-020-05004-4.

Femil, Jaculin, J. and Jaya, T. (2023) 'An efficient hybrid optimization for skin cancer detection using PNN classifier', *Computer Systems Science & Engineering*, Vol. 45, No. 3, pp.2919–2934.

Ferris, L.K., Harkes, J.A., Gilbert, B., Winger, D.G. and Satyanarayanan, M. (2015) 'Computer-aided classification of melanocytic lesions using dermoscopic images', *Journal of the American Academy of Dermatology*, November, Vol. 73, No. 5, pp.769–776.

Hussain, A.A., Themstrup, L., Nürnberg, B.M. and Jemec, G.B.E. (2016) 'Adjunct use of optical coherence tomography increases the detection of recurrent basal cell carcinoma over clinical and dermoscopic examination alone', *Photodiagnosis and Photodynamic Therapy*, June, Vol. 14, pp.178–184.

Jaimes, N., Marghoob, A.A., Rabinovitz, H., Braun, R.P. and Keir, J. (2015) 'Clinical and dermoscopic characteristics of melanomas on nonfacial chronically sun-damaged skin', *Journal of the American Academy of Dermatology*, June, Vol. 72, No. 6, pp.1027–1035.

Kahali, S., Sing, J.K. and Saha, P.K. (2018) 'A new entropy-based approach for fuzzy c-means clustering and its application to brain MR image segmentation', *Soft Computing*, October https://doi.org/10.1007/s00500-018-3594-y.

Kumar, M., Alshehri, M., Al Ghamdi, R. et al. (2020) 'A DE-ANN inspired skin cancer detection approach using fuzzy C-means clustering', *Mobile Netw. Appl*., Vol. 25, pp.1319–1329 https://doi.org/10.1007/s11036-020-01550-2.

Marchetti, M.A., Codella, N.C.F., Dusza, S.W. and Gutman, D.A. (2017) 'Results of the 2016 International Skin Imaging Collaboration International Symposium on Biomedical Imaging challenge: comparison of the accuracy of computer algorithms to dermatologists for the diagnosis of melanoma from dermoscopic images', *Journal of the American Academy of Dermatology*, 29 September, Vol. 78, No. 2, pp.270–277.

Mignion, L., Desmet, C.M., Harkemanne, E., Tromme, I., Joudiou, N., Wehbi, M., Baurain, J-F. and Gallez, B. (2022) 'Noninvasive detection of the endogenous free radical melanin in human skin melanomas using electron paramagnetic resonance (EPR)', *Free Radical Biology and Medicine*, Vol. 190, pp.226–233.

Mirbeik-Sabzevari, Li, S., Garay, E., Nguyen, H-T., Wang, H. and Tavassolian, N. (2019) 'Synthetic ultra-high-resolution millimeter-wave imaging for skin cancer detection', in *IEEE Transactions on Biomedical Engineering*, January, Vol. 66, No. 1, pp.61–71, DOI: 10.1109/TBME.2018.2837102.

Mohakud, R. and Dash, R. (2022) 'Designing a grey wolf optimization based hyper-parameter optimized convolutional neural network classifier for skin cancer detection', *Journal of King Saud University – Computer and Information Sciences*, Vol. 34, No. 8, pp.6280–6291.

Mohan, Y., Chee, S.S., Xin, D.K.P. and Foong, L.P. (2016) 'Artificial neural network for classification of depressive and normal in EEG', *2016 IEEE EMBS Conference on Biomedical Engineering and Sciences (IECBES)*.

Mondal, S., Sadhu, A.K. and Dutta, P.K. (2021) *Adaptive Local Ternary Pattern on Parameter Optimized-Faster Region Convolutional Neural Network for Pulmonary Emphysema Diagnosis*, 7 July, 18 July, 16 August, 23 August, DOI: 10.1109/ACCESS.2021.3105114.

Monika, M.K., Vignesh, N.A., Kumari, C.U., Kumar, M.N.V.S.S. and Lydia, E.L. (2020) 'Skin cancer detection and classification using machine learning', *Materials Today: Proceedings*, Vol. 33, pp.4266–4270.

Patil, R. and Bellary, S. (2022) 'Machine learning approach in melanoma cancer stage detection', *Journal of King Saud University – Computer and Information Sciences*, Vol. 34, No. 6, pp.3285–3293.

Pennisi, A., Bloisi, D.D., Nardi, D., Giampetruzzi, A.R. and Facchiano, A. (2016) 'Skin lesion image segmentation using Delaunay triangulation for melanoma detection', *Computerized Medical Imaging and Graphics*, September, Vol. 52, pp.89–103.

Rastghalam, R., Danyali, H., Helfroush, M.S., Celebi, M.E. and Mokhtari, M. (2021) 'Skin melanoma detection in microscopic images using HMM-based asymmetric analysis and expectation maximization', in *IEEE Journal of Biomedical and Health Informatics*, September, Vol. 25, No. 9, pp.3486–3497, DOI: 10.1109/JBHI.2021.3081185.

Senan, E.M. and Jadhav, M.E. (2021) 'Analysis of dermoscopy images by using ABCD rule for early detection of skin cancer', *Global Transitions Proceedings*, Vol. 2, No. 1, pp.1–7.

Tan, T.Y., Zhang, L. and Lim, C.P. (2019) 'Intelligent skin cancer diagnosis using improved particle swarm optimization and deep learning models', *Applied Soft Computing*, November, Vol. 84, Article 105725.

Thurnhofer-Hemsi, K. and Domínguez, E. (2021) 'A convolutional neural network framework for accurate skin cancer detection', *Neural Process Lett*., Vol. 53, pp.3073–3093 https://doi.org/10.1007/s11063-020-10364-y.

Togacar, M., Cömert, Z. and Ergen, B. (2021) 'Intelligent skin cancer detection applying autoencoder, MobileNetV2and spiking neural networks', *Chaos, Solutions and Fractals Nonlinear Science, and Non-equilibrium and Complex Phenomena*, Vol. 144, pp.1–8.

Tumpa, P.P. and Kabir, M.A. (2021) 'An artificial neural network based detection and classification of melanoma skin cancer using hybrid texture features', *Sensors International*, Vol. 2, pp.1–8.

Wang, Y., Louie, D.C., Cai, J., Tchvialeva, L., Lui, H., Wang, Z.J. and Lee, T.K. (2021) 'Deep learning enhances polarization speckle for in vivo skin cancer detection', *Optics and Laser Technology*, Vol. 140, pp.1–11.

Wei, L., Ding, K. and Hu, H. (2020) 'Automatic skin cancer detection in dermoscopy images based on ensemble lightweight deep learning network', in *IEEE Access*, Vol. 8, pp.99633–99647, DOI: 10.1109/ACCESS.2020.2997710.

Xie, F., Yang, J., Liu, J., Jiang, Z. and Wang, Y. (2020) 'Skin lesion segmentation using high-resolution convolutional neural network', *Computer Methods and Programs in Biomedicine*, April, Vol. 186, Article 105241.

Xue, G., Song, L., Sun, J. and Wu, M. (2011) *Hybrid Center-Symmetric Local Pattern for Dynamic Background Subtraction*, 978-1-61284-350-6/11/$26.00, IEEE.

Yang, S., Oh, B., Hahm, S., Chung, K-Y. and Lee, B-U. (2017) 'Ridge and furrow pattern classification for acral lentiginous melanoma using dermoscopic images', *Biomedical Signal Processing and Control*, February, Vol. 32, pp.90–96.

Zhang, B., Gao, Y., Zhao, S. and Liu, J. (2010) 'Local derivative pattern versus local binary pattern: face recognition with high-order local pattern descriptor', *IEEE Trans. on Image Processing*, Vol. 19, No. 2, pp.533–544.

Zhang, N., Cai, Y-X., Wang, Y-Y., Tian, Y-T. and Badami, B. (2020) 'Skin cancer diagnosis based on optimized convolutional neural network', *Artificial Intelligence in Medicine*, January, Vol. 102, Article 101756.

Zhao, S., Gao, Y. and Caelli, T. (2010) 'High-order circular derivative pattern for image representation and recognition', *Proc. 20th International Conference on Pattern Recognition*, pp.2246–2249.

Zhou, X., Lin, J., Zhang, Z., Shao, Z. and Liu, H. (2019) 'Improved itracker combined with bidirectional long short-term memory for 3D gaze estimation using appearance cues', *Neuro Computing*, 20 October, Vol. 390, pp.217–225.

Websites

https://en.wikipedia.org/wiki/Median_filter.

https://www.fc.up.pt/addi/ph2%20database.html.

Nomenclatures

Abbreviation	*Description*
AI	Artificial intelligence
CNN	Convolutional neural network
AOA	Arithmetic optimisation algorithm
ANN	Artificial neural network
CSAE	Convolutional sparse autoencoder
ALO	Ant lion optimisation
BOA	Butterfly optimisation
BRC-BOM	Battle royal customised butterfly optimisation model
Bi-LSTM	Bidirectional long short-term memory
CapsNet	Capsule network
DLCAL-SLDC	DL class attention layer CAD for skin lesion detection and classification
DNN	Deep neural network
FCM	Fuzzy means clustering
FF	FIREFLY
DL	Deep learning
GWO	Grey wolf optimisation
BRO	Battle royal optimisation
DCNN	Deep convolutional neural network
GLCM	Gray scale co-occurrence matrix
MGIA	Maximum gradient intensity algorithm
IMC	Information measures of correlation
MF	Median filtering
PSO	Particle swarm optimisation
TL	Transfer learning
LBP	Local binary pattern
LTP	Local ternary pattern
LDP	Local derivative patterns
OT	Otsu thresholding
NN	Neural networks
DE	Differential evolution
SSO	Swallow swarm optimisation
DS	Decision support
UV	Ultra violet
RNN	Recurrent neural network
ICS-LDPF	Improved centre symmetric local derivative pattern feature